

## Growth of calcium carbonate in the presence of Se(VI) in silica hydrogel

ÁNGELES FERNÁNDEZ-GONZÁLEZ<sup>1,\*</sup> AND LURDES FERNÁNDEZ-DÍAZ<sup>2,3</sup>

<sup>1</sup>Department of Geology, Universidad de Oviedo, 33005 Oviedo, Spain

<sup>2</sup>Department of Crystallography and Mineralogy, Universidad Complutense de Madrid, 28040 Madrid, Spain

<sup>3</sup>Instituto de Geociencias (CSIC, UCM), C/ José Antonio Novais 2, 28040 Madrid, Spain

### ABSTRACT

The element selenium has become a considerable environmental concern due its accumulation in aquifers on the one hand and the high radiotoxicity of its long-lived isotope <sup>79</sup>Se on the other hand. Se(VI) is the most mobile of the various Se cations. This study deals with the interaction of Se(VI) with rock-forming minerals (carbonates) to better understand how to mitigate the potential environmental hazards of Se.

The effect of Se(VI) on the crystallization of CaCO<sub>3</sub> at room temperature was studied using the silica hydrogel method. The CaCO<sub>3</sub> crystals obtained were characterized by X-ray powder diffraction, scanning electron microscopy and electron microprobe. The presence of Se(VI) in the growth medium has a clear effect on the polymorph selection of CaCO<sub>3</sub>, promoting the formation of vaterite and inhibiting that of aragonite. Se(VI) also affects the characteristics of calcite crystals, which show progressively more elongated habits and smaller sizes with increasing Se(VI) concentration in the growth medium. The effect of Se(VI) on both the polymorphic crystallization of CaCO<sub>3</sub> and the characteristics of calcite crystals shows features strikingly similar to those of other tetrahedral anionic groups like S(VI) and Cr(VI). This similarity extends to the amount of Se incorporated into the structure of the different CaCO<sub>3</sub> polymorphs, with calcite having Se contents up to 1200 ppm, vaterite up to 500 ppm, and aragonite growing virtually Se-free. The role of Se(VI) on the crystallization of CaCO<sub>3</sub> is discussed taking into consideration the physicochemical conditions in the growth medium at nucleation, which were modeled using the PHREEQ code for low-temperature aqueous geochemistry. The possible effect of the incorporation of the Se(VI) on the relative stability and, by extension, on the solubility of CaCO<sub>3</sub> polymorphs is also discussed.

**Keywords:** CaCO<sub>3</sub> polymorphism, Se(VI), CaCO<sub>3</sub> crystallization

### INTRODUCTION

Selenium is regarded as a trace element in the Earth's crust, commonly associated with metal-sulfide deposits. Although selenium is an element essential to most organisms, it becomes toxic to life when present in high concentrations (Spallholz 1994; Lemly 2004; Selinus 2005). Human activities such as mining, agriculture, and industrial production of pigments, glasses, and electronic devices have contributed to accelerate the mobilization of selenium, whose concentration in ground waters and soils has increased during the last decades in specific setups (Ong et al. 1997; Ryser et al. 2006). In fact, selenium has recently been identified as a major contaminant in aquatic ecosystems (Lenz and Lens 2008; May et al. 2008). This element is also relevant in the context of nuclear waste management due to the high radiotoxicity of its long-lived isotope <sup>79</sup>Se (Jörg et al. 2010). According to safety calculations assessments, <sup>79</sup>Se is expected to become one of the isotopes contributing most to the global radioactivity, as high concentrations of <sup>79</sup>Se could be released from waste disposals to the biosphere, causing serious long-term damage (Olyslaegers et al. 2005; Albrecht and Miquel 2010). The mobility of selenium under Earth surface conditions is strongly

affected by its tendency to oxidize. Both SeO<sub>3</sub><sup>2-</sup> and SeO<sub>4</sub><sup>2-</sup> [hereafter Se(IV) and Se(VI), respectively] are water-soluble (Elrashidi et al. 1987; Masscheleyn et al. 1990). While Se(IV) forms strong bonds with organic matter and oxide and hydroxide mineral surfaces, Se(VI) is not easily adsorbed nor incorporated into solid precipitates. As a result, Se(VI) can rapidly spread both in surface and ground waters (Zhang and Sparks 1990; Balistrieri and Chao 1987; Hayes et al. 1988; Elrashidi et al. 1987). Improving the current knowledge of the Se(VI) capacity to be incorporated into the structure of rock-forming minerals abundant in surface and sub-surface environments would help to develop efficient strategies to reduce the mobility of this pollutant.

In this work, we studied the crystallization of CaCO<sub>3</sub> in the presence of Se(VI). The experiments have been conducted using the double diffusion variant of the silica hydrogel method, which reproduces conditions similar to those existing in soils and sediments (Henish et al. 1986; Putnis et al. 1995). Our aim is to determine if Se(VI) can be incorporated in CaCO<sub>3</sub> crystals in amounts that could be relevant for the fate of this contaminant in natural environments. Because CaCO<sub>3</sub> has several polymorphs whose ability to incorporate Se(VI) can be expected to be different, special attention has been paid to the effect of Se(VI) on CaCO<sub>3</sub> polymorph selection and to the amount of Se incorporated in each polymorph. Finally, the effect of Se(VI) on

\* E-mail: mafernan@geol.uniovi.es

CaCO<sub>3</sub> crystallization is compared to the effect of Cr(VI), another contaminating ion with similar crystal-chemical characteristics.

## EXPERIMENTAL METHODS

### Crystal growth and characterization

The crystallization experiments were performed in a double diffusion system. The experimental setup is shown in Figure 1. It consists in a U-shaped tube made of glass whose two vertical reservoirs are filled with the reactant aqueous solutions, while the horizontal column (18 cm long) is occupied by silica hydrogel (Henisch 1988). The gel was prepared by acidification of a sodium silicate solution (Merck, density: 1.509 g/cm<sup>3</sup>; pH = 11.2) with 1 N HCl to a pH = 5.5. This solution was poured into the horizontal branch of the U-tube prior to polymerization. The silica hydrogel contains ~96.5 wt% water filling interconnecting micro-sized pores. One of the vertical branches (reservoir A) was filled with 10 cm<sup>3</sup> of a 0.3 M CaCl<sub>2</sub> aqueous solution and the other branch (reservoir B) was filled with 10 cm<sup>3</sup> of an aqueous solution with different ratios of Na<sub>2</sub>CO<sub>3</sub> and Na<sub>2</sub>SeO<sub>4</sub>. The simultaneous diffusion of Na<sub>2</sub>CO<sub>3</sub> and Na<sub>2</sub>SeO<sub>4</sub> from the same reservoir was preferred to the addition of Na<sub>2</sub>SeO<sub>4</sub> to the gel during its preparation to avoid possible gel dilution effects. All reagents were analytical grade. The concentration of the parent solutions in the different experiments are compiled in Table 1. The composition of these parent solutions was checked by inductively coupled plasma atomic emission spectroscopy (ICP-AES) with an iCAP 6000 (Thermo) plasma spectrometer.

Upon starting the experiments, reactants diffuse from the vertical branches and nucleation and growth eventually occurred by chemical reaction at a defined point within the gel. Crystal growth was monitored by optical microscopy to find the position of the first precipitate in the gel column and the time elapsed between the beginning of the experiment and the observation of the first crystallites under magnification 500×. This time will be referred to as waiting period (*t<sub>w</sub>*). The experiments were stopped two months after nucleation. Then, the crystals were extracted from the gel by dissolving it in a 1 M NaOH solution. The experiments were conducted at 25 ± 0.1 °C.

Crystals with representative morphologies were selected under a binocular stereomicroscope and studied using scanning electron microscopy in a JEOL 6610-LV microscope, equipped with energy-dispersive spectrometer Oxford INCA Energy 350 with X-max50 detector. This scanning electron microscope was also used to observe and analyze central sections of the crystals. Detailed quantita-

tive analyses of the crystals were obtained by electron microprobe (CAMEBAX SX-100). The identification of the solid phases was carried out by powder X-ray diffraction in a Philips PW1729-1710 diffractometer with graphite monochromator using CuKα-radiation.

### Modeling the physicochemical characteristics within the gel

The diffusion of the reactants through the gel leads to the development of concentration gradients, which evolve with time and position. Katsikopoulos et al. (2009) stated that the evolution of the reactant concentration in the column can be described by the one-dimensional algorithm

$$C(d,t + \Delta t) = \text{mix}fC(d - \Delta t) + (1 - 2\text{mix}f)C(d,t) + \text{mix}fC(d + \Delta t) \quad (1)$$

where *C* is the reactant concentration, *d* is the distance from the source reservoir, *t* is the diffusion time, and *mixf* is a mixing factor, which depends on the porosity ( $\phi = 1.19$ ), the effective tortuosity of the gel ( $\tau = 0.969$ ), and the diffusion coefficient of the reactant in water (*D<sub>w</sub>*). By combining this algorithm with a speciation model, the concentration profiles of the different chemical species in the gel column can be calculated for any diffusion time. In this work concentration profiles were calculated following this protocol and using the multicomponent-diffusion transport tool (MDT) of the geochemical code PHREEQC version 2.18.5570 (Parkhurst and Appelo 2003) and the llnl.dat thermodynamic database.

## RESULTS

### Nucleation time and location, crystallization sequence, and polymorph selection

In the experiments conducted the waiting period for nucleation (*t<sub>w</sub>*) ranged from 468 to 492 h, with no obvious correlation with the SeO<sub>4</sub>Na<sub>2</sub>-CO<sub>3</sub>Na<sub>2</sub> concentrations in reservoir B. In all the cases, the first nuclei appeared in a narrow region (~1 cm wide) of the diffusion column, located around 10 cm away from reservoir A. No significant differences regarding the total number of nuclei formed were detected in the different experiments.

After the first nucleation occurred, the length of the gel column occupied by crystals progressively increased, rightward at first and then leftward. As a result, three crystallization regions could be distinguished in the gel column: region 1, where the first nuclei formed; region 2, ~6 cm wide and located closer to reservoir B; and region 3, ~3 cm wide and located closer to reservoir A. The distribution of these regions within the gel column is depicted in Figure 2.

For a given experiment, each region was characterized by specific crystal morphologies and percentages of the three

**TABLE 1.** Initial concentration of the parent solutions

Experiment	Parent solutions		
	Reservoir A CaCl <sub>2</sub> (M ± 0.005)	Reservoir B Na <sub>2</sub> CO <sub>3</sub> (M ± 0.005)    Na <sub>2</sub> SeO <sub>4</sub> (M ± 0.005)	
E1	0.3	0.3	0.0
E2	0.3	0.3	0.01
E3	0.3	0.3	0.03
E4	0.3	0.3	0.05
E5	0.3	0.3	0.1
E6	0.3	0.3	0.3

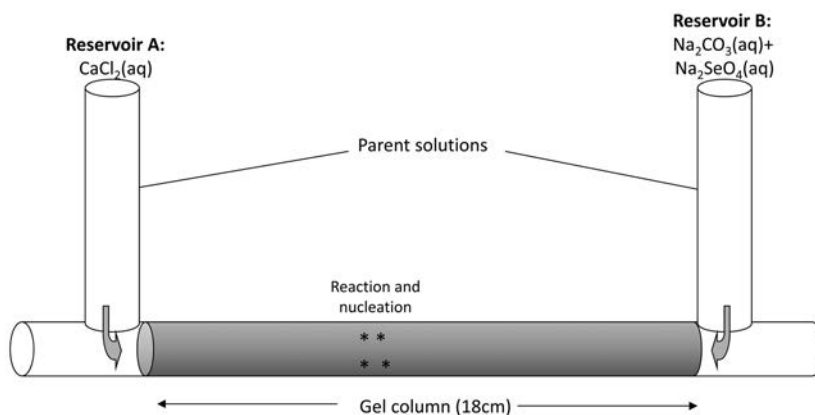


**FIGURE 1.** Experimental setup used for crystal growth.

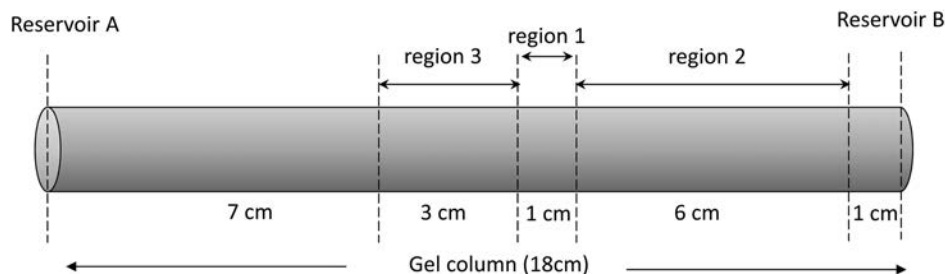


FIGURE 2. Distribution of crystallization regions in the gel column.

CaCO<sub>3</sub> polymorphs: calcite, aragonite, and vaterite. The different phases were initially identified using morphological criteria. This identification was subsequently confirmed by X-ray diffraction. The comparison between the results of different experiments evidenced that the presence of Se(VI) strongly affected both the polymorph selection and the crystal morphology. Although in all the experiments calcite always was the predominant CaCO<sub>3</sub> polymorph, the amount of vaterite strongly increased with Na<sub>2</sub>SeO<sub>4</sub> concentration in reservoir B. This effect was detected in both regions 1 and 2, although more pronounced in region 2 than in region 1. While no vaterite was detected in any region in experiment E1, where crystallization occurred in the absence of Se(VI), this phase constituted 56% of the precipitate in region 2 in experiment E6, where the initial Na<sub>2</sub>SeO<sub>4</sub> concentration in reservoir B was 0.3 M, the highest considered in this work. In contrast, no polymorph other than calcite was found in region 3 in any experiment. Aragonite crystals were only detected in region 1. The influence of an increasing initial Na<sub>2</sub>SeO<sub>4</sub> concentration in reservoir B on the formation of aragonite in region 1 seems to match a negative trend, with aragonite representing 15% of the precipitate in E1 (no Na<sub>2</sub>SeO<sub>4</sub> in reservoir B), which drops to a

6% in E2 (0.01 M Na<sub>2</sub>SeO<sub>4</sub> in reservoir B). A higher increase of the initial Na<sub>2</sub>SeO<sub>4</sub> concentration leads to no further decrease of the percentage of aragonite formed. These results are summarized in Table 2.

### Crystal morphology, size, and composition

The crystal morphology of the different CaCO<sub>3</sub> polymorphs is affected in different ways by the presence of SeO<sub>4</sub><sup>2-</sup> in the crystallization medium. The influence of SeO<sub>4</sub><sup>2-</sup> concentration on the morphology of both vaterite and aragonite is very limited to null. Vaterite crystals formed in experiments with different initial Na<sub>2</sub>SeO<sub>4</sub> concentration showed a limited variety of shapes, which ranged from spheres to aggregates consisting of lens-like individuals (see Figs. 3a and 3b). Similarly, aragonite appeared as spherulites or sheaf-like aggregates consisting of radiating needle-like crystals, irrespective of the initial Na<sub>2</sub>SeO<sub>4</sub> concentration. Figure 3c shows an example of an aragonite sheaf-like aggregate.

Calcite crystals, on the contrary, showed a large morphological variability, which correlates with both the location of the crystals within the gel column and the initial Na<sub>2</sub>SeO<sub>4</sub> concentration

TABLE 2. Percentages of calcite, vaterite, and aragonite (C, V, A) in the different regions of the U-tube

Experiment	Region 1			Region 2			Region 3			Total		
	C	V	A	C	V	A	C	V	A	C	V	A
E1	85±3	–	15±3	100±1	–	–	100±1	–	–	94±4	–	6±4
E2	94±2	–	6±2	84±5	16±5	–	100±1	–	–	85±7	8±3	2±1
E3	94±2	–	6±2	77±6	23±6	–	100±1	–	–	84±4	9±3	2±1
E4	93±2	1±1	6±1	70±7	30±7	–	100±1	–	–	80±5	18±4	2±1
E5	94±2	1±1	5±1	58±7	42±7	–	100±1	–	–	73±6	25±4	2±1
E6	93±2	2±1	5±1	44±5	56±5	–	100±1	–	–	60±7	38±6	2±1

Notes: The last three columns show the percentages in the entire tube. The percentage of calcite, aragonite, and vaterite was estimated by counting all the crystals inside the U-tube of each polymorph (identified with morphological criteria) under the binocular stereomicroscope at the end of each experiment, immediately before their extraction. The average number of crystals obtained in the experiments was ~200.

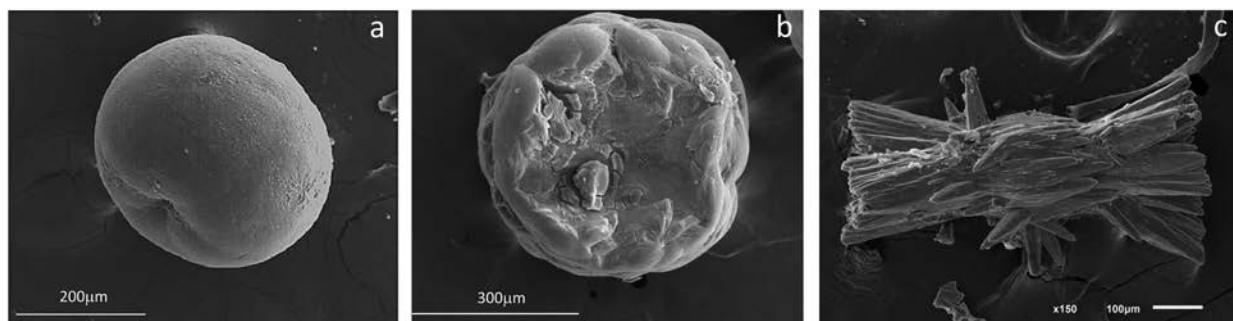


FIGURE 3. Morphologies of vaterite (a,b) and aragonite (c) grown in silica gel in the presence of Se(VI).

in reservoir B. For Se(VI)-free experiments (E1), calcite always appeared as rhombohedral single crystals. Small differences in shape were observed in crystals formed in the three different regions: The morphology of those crystals, which grew in region 1 were hopper or showed poorly developed dendritic branches, slightly differing from the typical rhombohedra. Crystals formed in region 3 were rhombohedra with flat faces bounded by either sharp (those converging in the threefold axis) or lobed edges (those not converging in the threefold axis). On the other hand, crystals formed in region 2 showed flat  $\{10\bar{1}4\}$  faces and sharp, well-defined edges. Representative examples of these crystals are shown in Figure 4.

When calcite grew in the presence of Se(VI), the morphological differences between crystals formed in the different regions within the gel column dramatically increased. The features of the calcite crystals formed in regions 1 and 3 coincided fairly well with those of the crystals grown in the same regions in Se(VI)-free experiments: dendritic to hopper crystals in region 1 and

rhomboheda with flat faces bounded by edges that are alternatively sharp and lobed in region 3 (Figs. 5a and 5b), and (Fig. 5c). In contrast, the morphology of calcite crystals grown in region 2 strongly differed from the typical  $\{10\bar{1}4\}$  rhombohedron. These crystals were elongated parallel to the *c*-axis, with rough, rounded surfaces in the prism region, poorly defined  $\{10\bar{1}4\}$ , and steeper rhombohedron faces and curved edges. Only those edges converging in the threefold axis were relatively straight and well defined. Figures 5d–5f show different examples of calcite crystals grown in region 2 in the presence of Se(VI), which are differently elongated and show different development of curved surfaces in the prism region. It is worth noting that significant differences in crystal size have also been observed between the calcite crystals grown both in Se(VI)-free experiments and in regions 1 and 3 in Se(VI)-bearing experiments, whose average sizes were around 1 mm when the experiments were terminated, and calcite crystals grown in region 2 in the presence of Se(VI), whose average size was around 400  $\mu\text{m}$ .

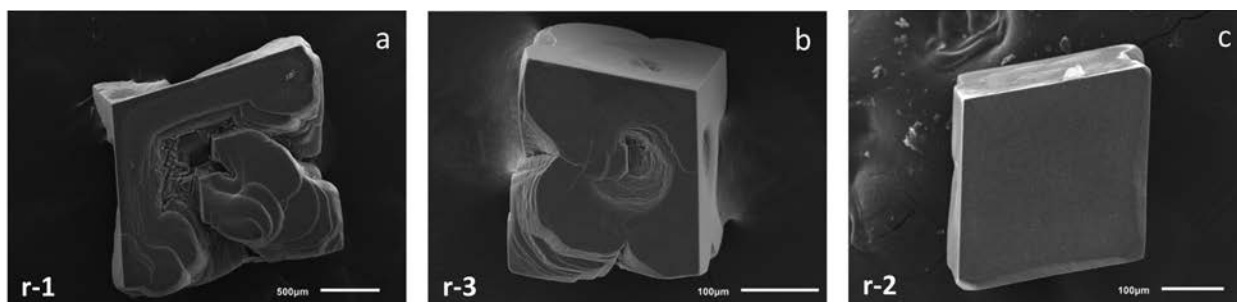


FIGURE 4. Morphologies of calcite observed for Se(VI)-free experiments in the different regions (r) of the gel column.

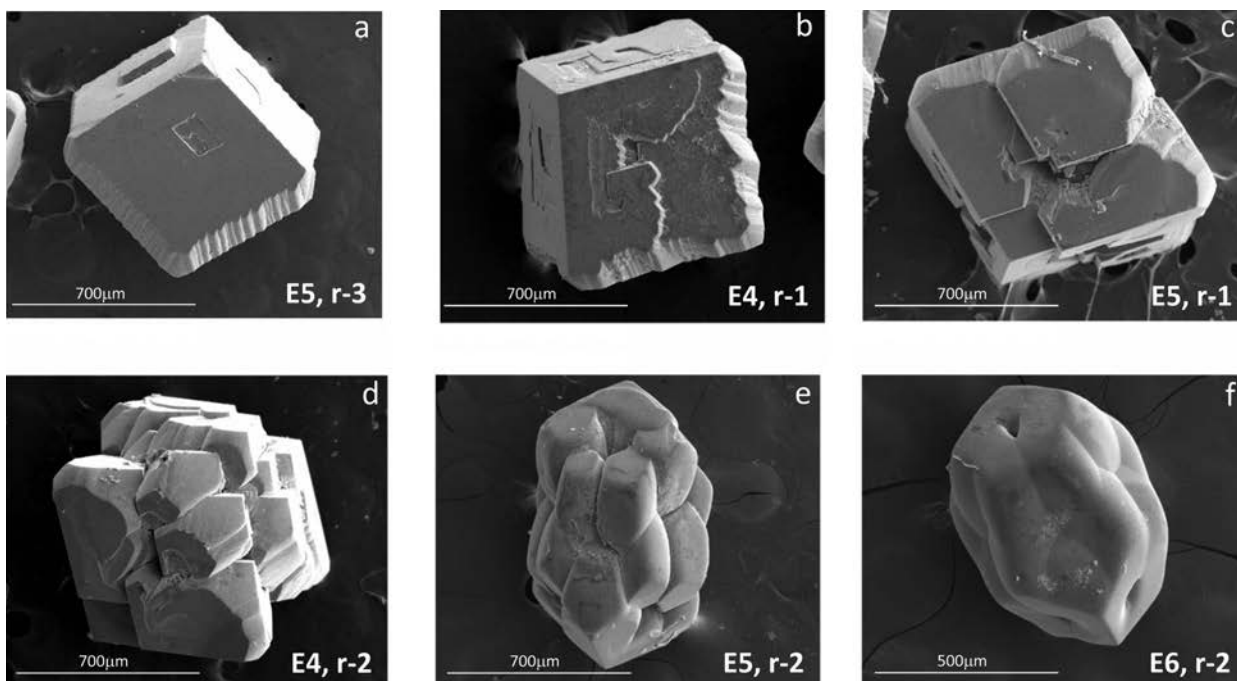


FIGURE 5. Morphologies of calcite grown in silica gel in the presence of Se(VI). The experiments in which the crystals were obtained (E) and the corresponding gel column regions (r) are indicated in each photo. The presence of Se(VI) in the aqueous solution increases form a to f.

To obtain information on the possible incorporation of Se(VI) in the structure of the different CaCO<sub>3</sub> polymorphs, a selection of vaterite and aragonite aggregates and calcite single crystals showing different length/width ratios were analyzed by electron microprobe. Significant differences in concentration of Se in-

corporated in the crystals composition were observed between the different polymorphs. In all the aragonite aggregates studied, Se contents were below the detection limit (100 ppm). Figure 6 shows an example of the Se content profile measured on an aragonite aggregate.

On the other hand, Se was detected both in vaterite and calcite. The Se content of vaterite aggregates ranged between 200 and 500 ppm, with a fairly homogenous distribution of Se from core to rim. Examples of Se content profiles in vaterite aggregates are shown in Figure 7.

Finally, calcite crystals showed a large variety of Se contents, depending on the region of the gel where they formed. Calcite crystals grown in region 3 showed the lowest Se contents, with concentrations ranging from 200 to 850 ppm and Se being more concentrated in the rim of the crystals. Selenium contents in crystals grown in region 1 varied from 400 to 650 ppm, with most samples showing a slight Se enrichment in the crystal core. Finally, the highest Se contents were found in the calcite crystals grown in region 2. These crystals showed cores with Se concentrations up to 1200 ppm, although the Se content rapidly decreased toward the rim. Figure 8 shows representative examples of calcite crystals formed in different regions of the gel column and their Se content profiles.

## DISCUSSION

### Physicochemical conditions at nucleation

The results of the experiments conducted show that the change in the initial Se(VI) concentration in reservoir B has no effect on the waiting time for nucleation or the first nuclei location in the gel column. In this type of experiments nucleation occurs as a consequence of the chemical reaction between dissolved

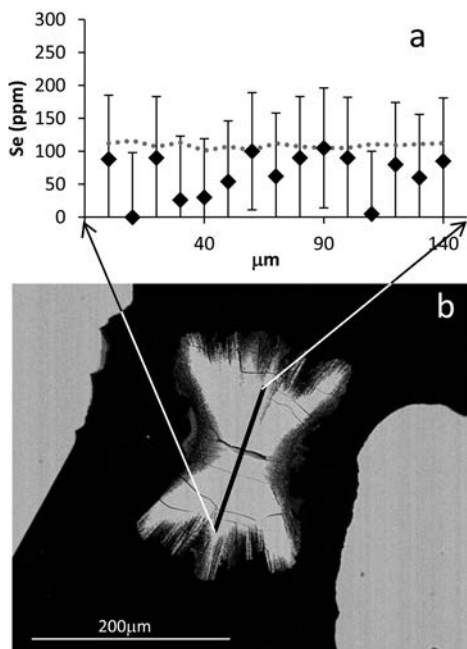


FIGURE 6. Se-content (a) determined by electronic microprobe analysis carried out on a central section of an aragonite aggregate (b). The dotted gray line on plot represents the detection limits in the Se-analysis.

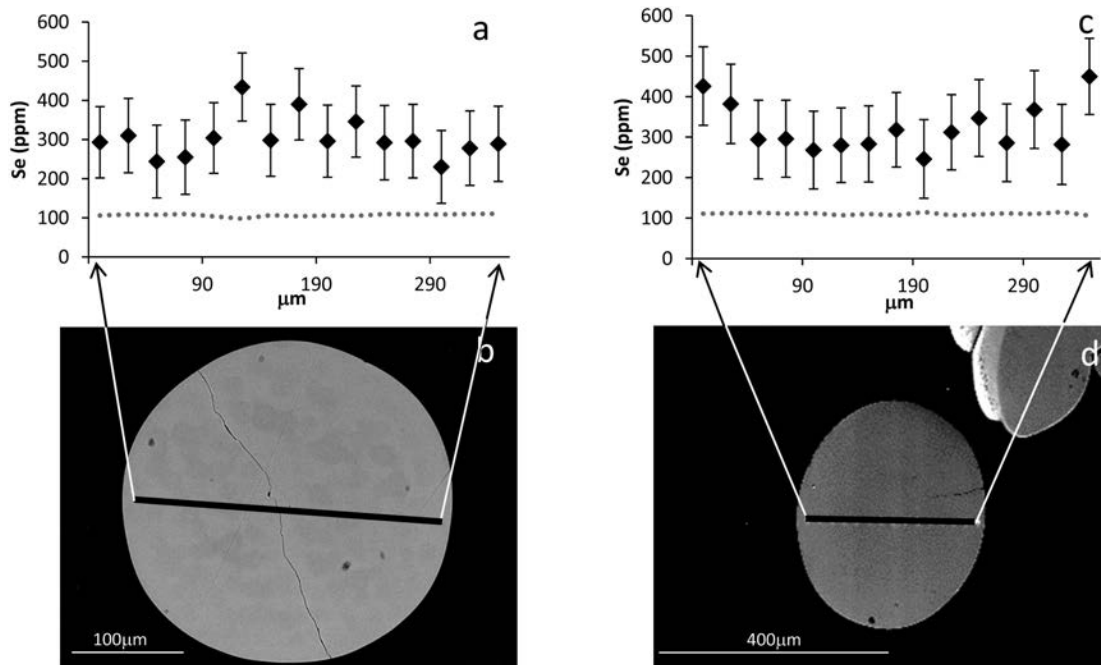
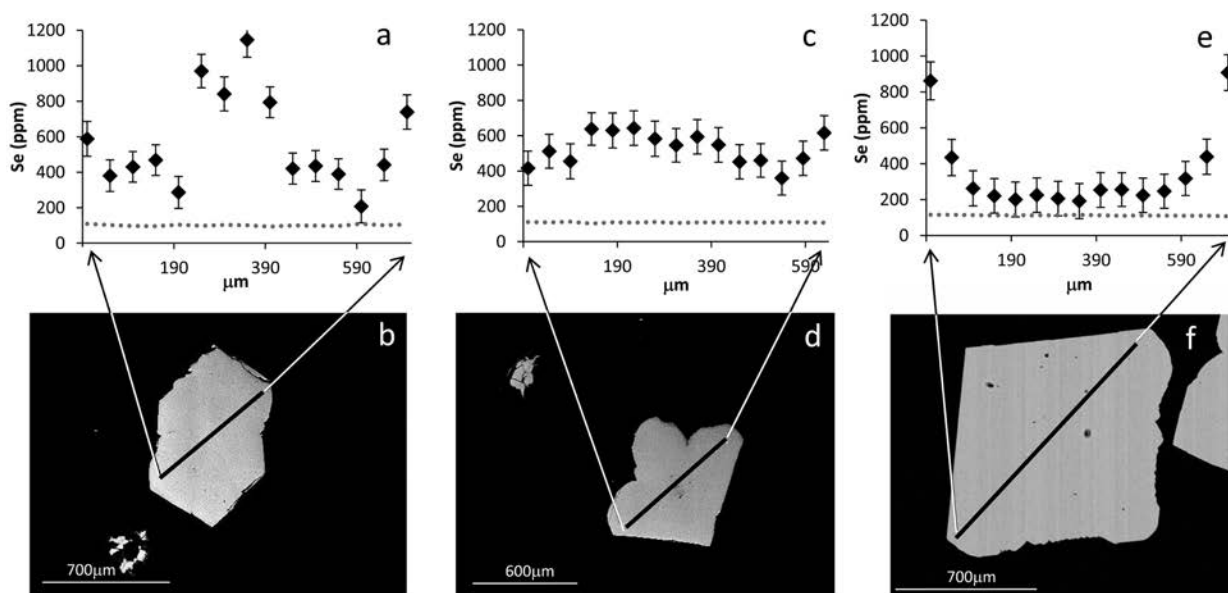


FIGURE 7. Se-content in vaterite determined by microprobe analysis (a, c). The dotted gray line on plots represents the detection limits in the Se-analysis. The analyses were carried out on central polished sections of the aggregates (b, d).



**FIGURE 8.** Se-content content in the calcite analyzed by electron microprobe (a, c, b). The dotted gray line represents the detection limits in the Se-analysis. The analyses were carried out on central polished sections of the shown crystals (b, d, f). Crystal b grew in region 2, crystal c in region 1, and crystal f in region 3.

species counter-diffusing from the reservoirs. At diffusion time = 0, the gel column is chemically homogeneous, but as soon as the experiment starts the counter-diffusion of the reactants leads to the development of concentration gradients that evolve with time and in space. Henish and Garcia-Ruiz (1986a, 1986b) proposed that the location of the first precipitate in counter-diffusion systems is controlled by the fulfillment of two main conditions: (1) the system has to be supersaturated, and (2) the activities of the anions and cations involved in the crystallization have to be similar (equality range condition). These requirements were later experimentally demonstrated (Prieto et al. 1989, 1991; Fernández-González et al. 1999). The actual supersaturation value at the nucleation time and location is determined by the boundary conditions, which in the present case are mainly defined by the length of the diffusion column and the initial concentration of the reactants in the reservoirs. The formation of CaCO<sub>3</sub> phases involves the reaction between Ca<sup>2+</sup> and CO<sub>3</sub><sup>2-</sup> ions. Since in all the experiments conducted the initial concentrations of CaCl<sub>2</sub> and Na<sub>2</sub>CO<sub>3</sub> in reservoir A and reservoir B, respectively, were identical and the waiting time for nucleation varied by <5%, no significant differences in supersaturation at the nucleation time and location is expected. The calculated saturation indexes with respect to the three CaCO<sub>3</sub> polymorphs calcite, aragonite, and vaterite at nucleation time and location show that this is the case. In all the experiments the system is supersaturated with respect to the three polymorphs, with saturation indexes around 2.7 for calcite, 2.5 for aragonite, and 2.1 for vaterite. Figure 9 depicts the distribution of Ca<sup>2+</sup>, CO<sub>3</sub><sup>2-</sup>, and SeO<sub>4</sub><sup>2-</sup> concentrations in the gel column at the nucleation time for experiments E1 and E6, calculated using PHREEQC. As can be seen, the concentrations of Ca<sup>2+</sup>, CO<sub>3</sub><sup>2-</sup>, and SeO<sub>4</sub><sup>2-</sup> are maximal close to the respective reservoirs, progressively decreasing with increasing distance. At the first precipitate location Ca<sup>2+</sup> and CO<sub>3</sub><sup>2-</sup> have the same value, i.e., Ca<sup>2+</sup>/CO<sub>3</sub><sup>2-</sup> ≈ 1, thereby fulfilling the reagents activity

equality requirement for nucleation postulated by Henish and García-Ruiz (1986a, 1986b).

As mentioned above, no significant differences in nucleation densities were observed in the different experiments. This is consistent with the fact that nucleation occurred at identical supersaturation in all the cases. It is also worth noting that the pH was identical in all the experiments with a value ~9.5. Since the SeO<sub>4</sub><sup>2-</sup>/CO<sub>3</sub><sup>2-</sup> ratio at nucleation time and location ranged from 0 in experiment E1 to ~1.6 in experiment E6, it can be concluded that the presence of Se(VI) in the crystallization medium does not inhibit CaCO<sub>3</sub> crystallization by reducing the total number of nuclei formed, at least within the range of Se(VI) concentrations explored.

### Polymorph selection

Since in all the experiments nucleation occurred under identical supersaturations with respect to the different CaCO<sub>3</sub> polymorphs, Se(VI) concentration has to be the factor controlling the proportion of precipitating polymorphs. From our results it can be concluded that Se(VI) promotes the metastable formation of vaterite while inhibiting the nucleation of calcite. This conclusion is supported by the fact that vaterite crystals nucleate in the region of the gel column where SeO<sub>4</sub><sup>2-</sup> concentration is higher, as shown in Figure 9. The effect of Se(VI) on the formation of aragonite is more complex: the amount of aragonite formed strongly decreases in the presence of a small concentration of Se(VI) but is no further reduced by an increase in Se(VI) concentration. The promotion of vaterite formation by Se(VI) is in good agreement with previously reported effects of tetrahedral anionic molecules like sulfate and chromate on the crystallization of CaCO<sub>3</sub>. For example, Fernández-Díaz et al. (2010) studied the temporal evolution of the ratio of CaCO<sub>3</sub> polymorphs formed in sulfate-bearing aqueous solutions. These authors reported that higher sulfate

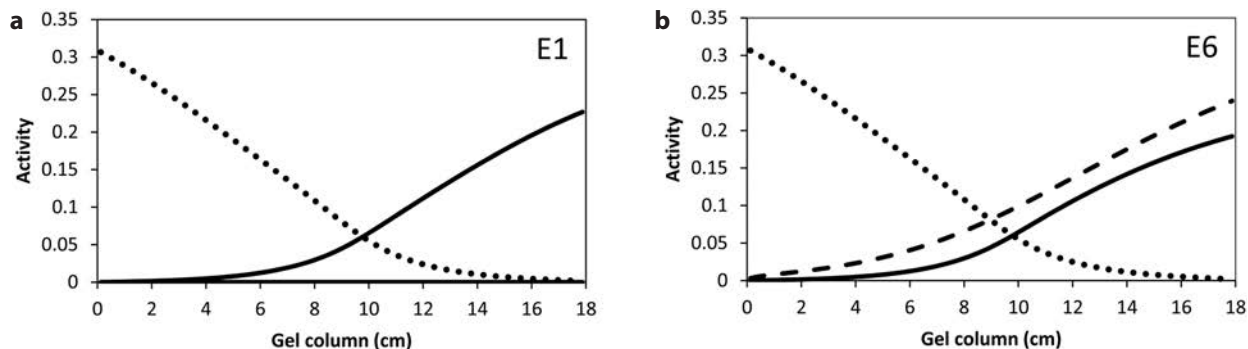


FIGURE 9. Activity for Ca<sup>2+</sup> (dotted line), CO<sub>3</sub><sup>2-</sup> (solid line), and SeO<sub>4</sub><sup>2-</sup> (dashed line) as modeled using PHREEQC for experiments E1 (a) and E6 (b).

contents in the solution lead to higher amounts of vaterite in the precipitate and a progressively more sluggish transformation of vaterite into calcite (Fernández-Díaz et al. 2009, 2010). A direct relationship between dissolved chromate and the amount of vaterite in CaCO<sub>3</sub> precipitates has also been reported (Hua et al. 2007; Sánchez-Pastor et al. 2011). Moreover, increasing concentrations of chromate progressively delays the transformation of vaterite into calcite (Cruz et al. 2011). Bots et al. (2011) have highlighted the fact that sulfate can play a complex role in CaCO<sub>3</sub> polymorphism decreasing the Mg/Ca ratio at which the polymorph precipitating from seawater switches from calcite to aragonite. Although carbonate is a triangular planar anionic molecule and large distortions or disruption of local structure would be required to accommodate its substitution by tetrahedral anions, numerous experimental evidences support that sulfate and chromate substitute for carbonate in natural and synthetic calcites (Busenberg and Plummer 1985; Frisia et al. 2005; Sánchez-Pastor 2011). Such substitutions were proposed on the basis of XANES and EXAFS measurements on calcite single crystals (Staudt et al. 1994; Tang et al. 2007). Recently, computational modeling showed the viability of a certain degree of carbonate substitution by sulfate in the structure of CaCO<sub>3</sub> polymorphs, indicating that this substitution is energetically favorable in vaterite, slightly unfavorable in calcite and very unfavorable in aragonite (Fernández-Díaz et al. 2010). According to these previous results, the effect of sulfate on the polymorph selection of CaCO<sub>3</sub> is related to a differential solubility behavior of the three CaCO<sub>3</sub> polymorphs as they incorporate sulfate. A similar explanation, combined with specific effects on the surface of the different polymorphs has been proposed for the influence of chromate on CaCO<sub>3</sub> crystallization (Sánchez-Pastor 2011). In the case of selenate, synchrotron radiation-based studies provided direct evidence that this anion substitutes for carbonate in the structure of calcite (Lamble et al. 1995; Reeder et al. 1994). Selenate is larger than sulfate and almost identical to chromate. From geometrical considerations, it can be expected that the incorporation of selenate into CaCO<sub>3</sub> polymorphs would be similar to that of chromate but less than that of sulfate. Accordingly, the effect of selenate on CaCO<sub>3</sub> crystallization should be similar to the effect of chromate and less intense than the effect of sulfate. Indeed, our results confirm that selenate promotes the formation

of vaterite in a similar extent as chromate, but not as strongly as sulfate. This is in contrast with the inhibiting effect of selenate on the formation of aragonite, whose nucleation is promoted by chromate and seems to be little affected by sulfate unless in combination with other ions. Understanding the differential effect of tetrahedral anions on aragonite nucleation will require carrying out further research.

#### Polymorph compositions

The differential incorporation of Se in CaCO<sub>3</sub> polymorphs is in good agreement with data in the literature regarding the incorporation of other tetrahedral anionic molecules. For example, it has been reported that while the sulfate content of biogenic aragonite never exceeds 6000 ppm (Land and Hoops 1973), it can reach values of several units weight percent in biogenic and inorganic calcites (Busenberg and Plummer 1985). On the other hand, the Raman analysis of aragonite grown in silica gel in the presence of chromate showed no vibrational bands, which could be assigned to the chromate group. These bands were present both in calcite and vaterite (Sánchez-Pastor et al. 2011), showing a higher intensity in calcite. In addition, microprobe analyses of these calcite crystals yielded Cr contents in the range between 1500 and 6000 ppm. This differential incorporation is in agreement with the conclusion derived from computational modeling that the incorporation of tetrahedral anionic molecules differentially affects the energetics of the different CaCO<sub>3</sub> polymorphs (Fernández-Díaz et al. 2010), with this incorporation being very unfavorable in the case of aragonite and less so in calcite and vaterite.

The difficulty of incorporating Se(VI) into the structure of aragonite could be the reason for the reduction of the amount of aragonite formed in experiments E2 to E6, where crystallization occurred in the presence of Se(VI), in comparison to the amount of aragonite formed in E1, in the absence of Se(VI). The lower Se content of vaterite crystals in comparison to calcite in region 2 could be explained by the fact that vaterite crystals form earlier during the experiment. It is worth noting that the evolution of SeO<sub>4</sub><sup>2-</sup>/CO<sub>3</sub><sup>2-</sup> ratio is the result of the coupling between mass transfer from the reservoirs and reagent consumption by the growing crystals. It can be assumed that the diffusion of SeO<sub>4</sub><sup>2-</sup> and CO<sub>3</sub><sup>2-</sup> yields no significant differences. Since the consumption of CO<sub>3</sub><sup>2-</sup> to form of vaterite crystals is always

higher than the consumption of  $\text{SeO}_4^{2-}$ , the  $\text{SeO}_4^{2-}/\text{CO}_3^{2-}$  ratio must increase as growth proceeds. Therefore, calcite crystals will nucleate in the presence of higher  $\text{SeO}_4^{2-}/\text{CO}_3^{2-}$  ratios than vaterite aggregates.

The Se contents of calcite crystals formed in the different regions correlates well with the Se(VI) concentration in the growth medium as shown Figure 9.  $\text{SeO}_4^{2-}$  profiles were calculated at the nucleation time and it is not possible to estimate how these profiles evolve with time due to the diffusion disturbance resulting from the growth of the first nuclei. However, these profiles can be used as a reference of the distribution of  $\text{SeO}_4^{2-}$  concentrations in the gel column. As can be seen, at nucleation time the highest  $\text{SeO}_4^{2-}$  concentration corresponds to region 2, followed by region 1 and, finally, region 3, with the lowest  $\text{SeO}_4^{2-}$  concentration, in agreement with the respective Se content of the crystals.

Figure 10 shows the calculated ideal distribution of  $\text{Ca}^{2+}$ ,  $\text{CO}_3^{2-}$ , and  $\text{SeO}_4^{2-}$  concentrations and the pH in the gel column 636 h after the beginning of experiment E6, assuming that no nucleation occurred. This time is 168 h longer than the actual nucleation time. The ideal profile of  $\text{SeO}_4^{2-}$  in Figure 10 can be considered realistic due to the scarce incorporation of  $\text{SeO}_4^{2-}$  into crystals formed in region 1. However, since all nucleated crystals represent a sink for  $\text{Ca}^{2+}$  and  $\text{CO}_3^{2-}$  ions, ideal profiles for these ions in Figure 10 will significantly differ from the real ones. Indeed, the consumption of  $\text{Ca}^{2+}$  and  $\text{CO}_3^{2-}$  due to the growth of crystals in region 1 will differently disrupt the subsequent evolution of the concentration of these ions in regions 2 and 3. In region 2, closer to reservoir B ( $\text{CO}_3^{2-}$  source), diffusion dis-

turbances will mainly affect the  $\text{Ca}^{2+}$  concentration, which will be lower than predicted in an ideal situation. On the contrary, in region 3, closer to reservoir A ( $\text{Ca}^{2+}$  source), a lower concentration than predicted is expected for  $\text{CO}_3^{2-}$ . Similarly, because the pH evolution in the gel column is coupled to the concentration of  $\text{CO}_3^{2-}$ , the characteristics of the pH profile can be considered unrealistic in the gel column from region 1 to reservoir A, where lower values should be expected.  $\text{CaCO}_3$  crystallization requires high pHs to occur because of the pH-dependent distribution of carbonate species. Therefore, the disruption of  $\text{CO}_3^{2-}$  diffusion has a stronger influence on the supersaturation profile than that of  $\text{Ca}^{2+}$ . This can explain why the widening of the length of the gel column occupied by crystals preferentially occurs toward the reservoir B. Since the incorporation of impurities into crystal structure is favored by high-supersaturation levels (Prieto et al. 1997), a lower supersaturation might also explain that almost no  $\text{SeO}_4$  is incorporated in the crystals formed in region 3.

### Calcite habit evolution

The spatial and temporal evolution of the calcite crystal habits in Se(VI)-free experiments can be explained based on both supersaturation evolution and the specific characteristics of the calcite structure (Fernández-González et al. 1999, 2006). Dendritic crystals in region 1 form first, most likely under higher supersaturation. The reagent consumption due to the growth of crystals in region 1 determines that the nucleation and growth of crystals in regions 2 and 3 occur at progressively lower supersaturations. As a result, the predominant growth mechanism evolves from adhesive to two-dimensional nucleation and,

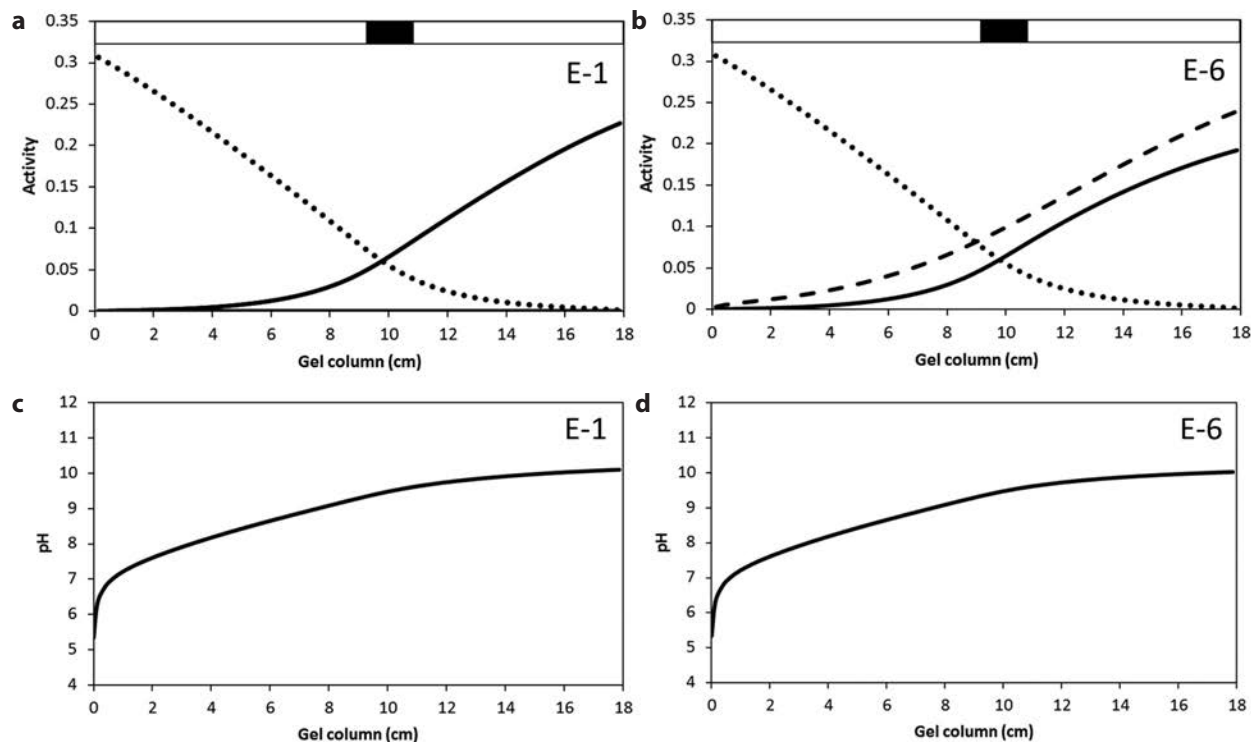


FIGURE 10. Activity for  $\text{Ca}^{2+}$  (dotted line),  $\text{CO}_3^{2-}$  (solid line) and  $\text{SeO}_4^{2-}$  (dashed line) (a,c) and (b,d) pH profiles as modeled using PHREEQC for experiments E1 and E6 considering 636 h diffusion time and no disruption of the diffusion progress due to crystallization.

finally, spiral growth, explaining the parallel evolution from dendritic morphologies to hopper crystals and well-developed rhombohedra. It is worthwhile noting that calcite dendritic and hopper crystals are characterized by a more or less marked cleft in their equatorial region, which results from a different development of the edges converging in the threefold axis in comparison to those non-converging (Figs. 4a and 4b). All these edges are parallel to the  $\langle 441 \rangle$  PBC (Heijnen 1985). However, the orientation of the carbonate groups in the calcite structure determines that parallel growth step edges, which advance in opposite directions contain growth sites with non-equivalent geometries (Paquette and Reeder 1995; Reeder and Rakovan 1999; Staudt et al. 1994). This non-equivalence determines that, as has extensively been shown by molecular scale observations (Astilleros et al. 2006; Hillner et al. 1992; Jordan and Rammensee 1998; Teng et al. 2000), opposing steps advance at very different rates, which in turn can explain the different development of parallel edges bounding  $\{10\bar{1}4\}$  faces in calcite (Fernández-Díaz et al. 2006).

A similar combination of the change in supersaturation and the specific characteristics of the  $\langle 441 \rangle$  edges can explain the morphological evolution of calcite crystals formed in Se(VI)-bearing gels in regions 1 and 3 and can also explain the alternation of sharp and lobbed edges bounding the  $\{10\bar{1}4\}$  faces and the marked equatorial cleft in crystals formed in region 2. However, these crystals are progressively more elongated along the  $c$  axis due to the development of curved surfaces in the prism region as the concentration of Se(VI) in reservoir B increases. This characteristic is also shown by crystals formed in the presence of other tetrahedral anions like  $\text{SO}_4^{2-}$ ,  $\text{CrO}_4^{2-}$ , or  $\text{HPO}_4^{2-}$  (Fernández-Díaz 2010; Sánchez-Pastor et al. 2011; Suzuki et al. 1986). The effect of these anions on calcite habits has been related to selective binding on sites in prism surfaces (Parker et al. 1993; Titiloye et al. 1993).

In summary, the experiments presented in this work show that the presence of Se(VI) influences the crystallization of calcium carbonate precipitated from aqueous solutions. The incorporation of selenate in the CaCO<sub>3</sub> crystals is limited, but it affects both the stability of the different CaCO<sub>3</sub> polymorphs and the morphology and size of the calcite crystals. Specifically, the presence of Se(VI) seems to promote the stabilization of vaterite and tends to inhibit the nucleation of aragonite. The tetrahedral anion  $\text{SeO}_4^{2-}$  can be incorporated into the structure of calcite and vaterite when they precipitate far from equilibrium, but no Se was observed in aragonite grown under identically high-supersaturation conditions. The modification of the solubility of the impure phases with respect to pure calcite and vaterite might explain the effect of selenate on the polymorphism of CaCO<sub>3</sub>. Calcite crystals grown from aqueous solutions in the presence of Se(VI), tend to develop elongated morphologies and crystal sizes decrease when the selenium concentration increases.

#### ACKNOWLEDGMENTS

This research was supported by MICINN-Spain, under grants CGL2010-20134-C02-01 and CGL2010-20134-C02-02 and by the German Federal Ministry of Education and Research (ImmoRad: Basic research on Immobilization of long-lived Radionuclides by interaction with relevant secondary repository-phases). The authors wish to thank the editors D. Vielzeuf and M. Kunz and the anonymous reviewers whose comments and suggestions have improved this work.

#### REFERENCES CITED

- Albrecht, A., and Miquel, S. (2010) Extension of sensitivity and uncertainty analysis for long term dose assessment of high-level nuclear waste disposal sites to uncertainties in the human behavior. *Journal of Radioactivity*, 101, 55–67.
- Astilleros, J.M., Pina, C.M., Fernández-Díaz, L., and Putnis, A. (2006) Nanoscale phenomena during the growth of solid solutions on calcite  $\{10\bar{1}4\}$ . *Chemical Geology*, 225, 322–335.
- Balistreri, L.S., and Chao, T.T. (1987) Selenium adsorption by goethite. *Soil Science Society of America Journal*, 51, 1145–1151.
- Bots, P., Benning, L.G., Rickaby, R.E.M., and Shaw, S. (2011) The role of SO<sub>4</sub> in the switch from calcite to aragonite seas. *Geology*, 39, 331–334.
- Busenberg, E., and Plummer, N. (1985) Kinetic and thermodynamic factors controlling the distribution of SO<sub>4</sub><sup>2-</sup> and Na<sup>+</sup> in calcites and selected aragonites. *Geochimica et Cosmochimica Acta*, 49, 713–725.
- Cruz, J., Sánchez-Pastor, N., Gigler, A.M., and Fernández-Díaz, L. (2011) Vaterite (CaCO<sub>3</sub>) stability in the presence of chromate. *Spectroscopy Letters*, 44, 495–499.
- Elrashidi, M.A., Adriano, D.C., Workman, S.M., and Lindsay, W.L. (1987) Chemical-equilibria of selenium in soils—a theoretical development. *Soil Science*, 144, 141–152.
- Fernández-Díaz, L., Astilleros, J.M., and Pina, C.M. (2006) The morphology of calcite crystals grown in a porous medium doped with divalent cations. *Chemical Geology*, 225, 314–321.
- Fernández-Díaz, L., Pina, C.M., Astilleros, J.M., and Sánchez-Pastor, N. (2009) The carbonation of gypsum: Pathways and pseudomorph formation. *American Mineralogist*, 94, 1223–1234.
- Fernández-Díaz, L., Fernández-González, A., and Prieto, M. (2010) The role of sulfate groups in controlling CaCO<sub>3</sub> polymorphism. *Geochimica et Cosmochimica Acta*, 74, 6064–6076.
- Fernández-González, A., Prieto, M., Putnis, A., and López-Andrés, S. (1999) Concentric zoning patterns in crystallizing (Cd,Ca)CO<sub>3</sub> solid solutions from aqueous solutions. *Mineralogical Magazine*, 63, 331–343.
- Frisia, S., Borsato, A., Fairchild, I.J., and Susini, J. (2005) Variations in atmospheric sulphate recorded in stalagmites by synchrotron micro-XRF and XANES analyses. *Earth and Planetary Science Letters*, 235, 729–740.
- Hayes, K.F., Papelis, C., and Leckie, J.O. (1988) Modelling ionic strength effects on anion adsorption at hydrous oxide/solution interfaces. *Journal of Colloid and Interface Science*, 125, 717–726.
- Heijnen, W.M.M. (1985) The morphology of gel grown calcite. *Neues Jahrbuch für Mineralogie, Monatshefte*, 8, 357–362.
- Henisch, H.K. (1988) *Crystals in gels and Liesegang rings*. Cambridge University Press, U.K.
- Henisch, H.K., and García-Ruiz, J.M. (1986a) Crystal growth in gels and Liesegang ring formation: I. Diffusion relationships. *Journal of Crystal Growth*, 75, 195–202.
- (1986b) Crystal growth in gels and Liesegang ring formation: II. Crystallization criteria and successive precipitation. *Journal of Crystal Growth*, 75, 203–211.
- Hillner, P.E., Gratz, A.J., Manne, S., and Hansma, P.K. (1992) Atomic-scale imaging of calcite growth and dissolution in real time. *Geology*, 20, 359–362.
- Hua, B., Deng, B.L., Thorton, E.C., Yang, J., and Amonette, J.E. (2007) Incorporation of chromate into calcite structure during coprecipitation. *Water, Air and Soil Pollution*, 179, 381–390.
- Jordan, G., and Rammensee, W. (1998) Dissolution rates of calcite (10 $\bar{1}4$ ) surfaces obtained by scanning force microscopy: Microtopography-based dissolution kinetics on surfaces with anisotropic velocities. *Geochimica et Cosmochimica Acta*, 62, 941–947.
- Jörg, G., Bühnenmann, R., Hollas, S., Kivel, N., Kossert, K., Van Winkel, S., and Gostomski, C.L. (2010) Preparation of radiochemically pure <sup>79</sup>Se and highly precise determination of its half-life. *Applied Radiation and Isotopes*, 68, 2339–2351.
- Katsikopoulos, D., Fernández-González, A., and Prieto, M. (2009) Crystallization behaviour of the (Mn,Ca)CO<sub>3</sub> solid solution in silica gel: Nucleation, growth and zoning phenomena. *Mineralogical Magazine*, 73, 269–284.
- Lamble, G.M., Lee, J.F., Staudt, W.J., and Reeder, R.J. (1995) Structural studies of selenate incorporation into calcite crystals. *Physica B*, 208–209, 589–590.
- Land, L.S., and Hoops, G.K. (1973) Sodium in carbonate sediments and rocks: a possible index to salinity of diagenetic solutions. *Journal of Sedimentary Petrology*, 43, 614–617.
- Lemly, A.D. (2004) Aquatic selenium pollution is a global environmental safety issue. *Ecotoxicology and Environmental Safety*, 9, 44–56.
- Lenz, M., and Lens, P.N.L. (2008) The essential toxin: the changing perception of selenium in environmental sciences. *Science of the Total Environment*, 407, 3620–3633.
- Masscheleyn, P.H., Delaune, R.D., and Patrick, W.H. (1990) Transformations of selenium as affected by sediment oxidation reduction potential and pH. *Environmental Science and Technology*, 24, 91–96.
- May, T.W., Fairchild, J.F., Petty, J.D., Walther, M.J., Lucero, J., Delvaux, M.,

- Manring, J., and Armbruster, M. (2008) An evaluation of selenium concentrations in water, sediment, invertebrates, and fish from the Solomon River Basin. *Environmental Monitoring and Assessment*, 137, 213–232.
- Olyslaegers, G., Zeevaert, T., Pinedo, P., Simon, I., Prohl, G., Kowe, R., Chen, Q., Mobbs, S., Bergstrom, U., Hallberg, B., Katona, T., Eged, K., and Kanyar, B. (2005) A comparative radiological assessment of five European biosphere systems in the context of potential contamination of well water from the hypothetical disposal of radioactive waste. *Journal of Radiological Protection*, 25, 375–391.
- Ong, C.G., Herber, M.J., Dahlagren, R.A., and Tanji, K.K. (1997) Trace elements (Se, As, Mo, B) contamination of evaporates in hypersaline agricultural evaporation ponds. *Environmental Science and Technology*, 31, 831–836.
- Paquette, J., and Reeder, R.J. (1995) Relationships between surface structure, growth mechanism, and trace element incorporation in calcite. *Geochimica et Cosmochimica Acta*, 59, 735–749.
- Parker, S.C., Titiloye, J.O., and Watson, G.W. (1993) Molecular modelling of carbonate minerals: Studies of growth and morphology. *Philosophical Transactions of the Royal Society of London A*, 344, 37–48.
- Parkhurst, D.L., and Appelo, C.A.J. (2003) User's guide to PHREEQC (Version 2)—A computer program for Speciation, Batch-Reaction, One-Dimensional Transport and Inverse Geochemical Calculations. U.S. Geological Survey Water-Resources Investigations Report 99-4259, 310 pp., Washington D.C.
- Prieto, M., Fernández-Díaz, L., and López-Andrés, S. (1989) Supersaturation evolution and first precipitate location in crystal growth in gels; Application to barium and strontium carbonates. *Journal of Crystal Growth*, 98, 447–460.
- (1991) Spatial and evolutionary aspects of nucleation in diffusing-reacting systems. *Journal of Crystal Growth*, 108, 770–778.
- Prieto, M., Fernández-González, A., Putnis, A., and Fernández-Díaz, L. (1997) Nucleation, growth, and zoning phenomena in crystallizing (Ba,Sr)CO<sub>3</sub>, Ba(SO<sub>4</sub>,CrO<sub>4</sub>), (Ba,Sr)SO<sub>4</sub>, and (Cd,Ca)CO<sub>3</sub> solid solutions from aqueous solutions. *Geochimica et Cosmochimica Acta*, 61, 3383–3397.
- Putnis, A., Prieto, M., and Fernández-Díaz, L. (1995) Fluid supersaturation and crystallization in porous media. *Geological Magazine*, 132, 1–13.
- Reeder, R.J., and Rakovan, J. (1999) Surface structural controls on trace element incorporation during crystal growth. In B. Jamtveit and P. Meakin, Eds., *Growth, Dissolution and pattern formation in geosystems*, p.143–162. Kluwer Academic Publishers, Dordrecht, Netherlands.
- Reeder, R.J., Lamble, G., Lee, J.F., and Staudt, W. (1994) Mechanism of SeO<sub>4</sub><sup>2-</sup> substitution in calcite: An XAFS study. *Geochimica et Cosmochimica Acta*, 58, 5639–5646.
- Ryser, A.L., Strawn, D.G., Marcus, M.A., Fakra, S., Johnson-Maynard, J.L., and Möller, G. (2006) Microscopically focused synchrotron X-ray investigation of the speciation in soils developing on reclaimed mine lands. *Environmental Science and Technology*, 40, 462–467.
- Sánchez-Pastor, N., Gigler, A.M., Cruz, J.A., Park, S.H., Jordan, G., and Fernández-Díaz, L. (2011) Growth of calcium carbonate in the presence of Cr(VI). *Crystal Growth and Design*, 11, 3081–3089.
- Selinus, O. (2005) *Essentials of Medical Geology*. Elsevier Academic Press, London.
- Spallholz, J.E. (1994) On the nature of selenium toxicity and carcinostatic activity. *Biology and Medicine*, 17, 45–64.
- Staudt, W.J., Reeder, R.J., and Schoonen, W.A.A. (1994) Surface structural controls on compositional zoning of SO<sub>4</sub><sup>2-</sup> and SeO<sub>4</sub><sup>2-</sup> in synthetic calcite single crystals. *Geochimica et Cosmochimica Acta*, 58, 2087–2098.
- Suzuki, T., Inomata, S., and Sawada, K. (1986) Adsorption of phosphate on calcite. *Journal of the Chemical Society, Faraday Transactions*, 82, 1733–1743.
- Tang, Y., Elzinga, E.J., Lee, Y.J., and Reeder, R.J. (2007) Coprecipitation of chromate with calcite: Batch experiments and X-ray absorption spectroscopy. *Geochimica et Cosmochimica Acta*, 71, 1480–1493.
- Teng, H., Dove, P.M., and De Yoreo, J.J. (2000) Kinetics of calcite growth: Surface processes and relationships to macroscopic rate laws. *Geochimica et Cosmochimica Acta*, 64, 2255–2266.
- Titiloye, J.O., Parker, S.C., and Mann, S. (1993) Atomistic simulation of calcite surfaces and the influence of growth additives on their morphology. *Journal of Crystal Growth*, 131, 533–545.
- Zhang, P., and Sparks, D.L. (1990) Kinetics of selenate and selenite adsorption/desorption at the goethite/water interface. *Environmental Science and Technology*, 24, 1848–1856.

MANUSCRIPT RECEIVED NOVEMBER 6, 2012

MANUSCRIPT ACCEPTED JUNE 4, 2013

MANUSCRIPT HANDLED BY DANIEL VIELZEUF